Journal of Computational and Experimental Science (JCES)
ISSN Print: XXXX | ISSN Online: XXXX
Volume 1, Number 1, 2026, Pages 76-88
Journal Home Page: https://journals.airsd.org/index.php/jces

Hybrid Plasmonic Modes In Graphene-Loaded Waveguide Surrounded By Insb And Magnetized Plasma Layers

Sanam saleem[1], Maham Nadeem[1], Abdul Ghaffar[1*], Muhammad Umair[1*]

[1] Department of Physics, University of Agriculture, Faisalabad, Pakistan

ARTICLE INFO

Article History:
Received: April 15, 2026
Revised: May 17, 2026
Accepted: June 05, 2026
Available Online: June 11, 2026

Keywords:
Plasmonic Modes, Graphene, Waveguide, Magnetized Plasma, Temperature Sensitive Material

Corresponding Author:
Muhammad Umair
Email: rumair.uaf@gmail.com
Abdul Ghaffar
Email: aghaffar16@uaf.edu.pk

ABSTRACT

In this paper, hybrid plasmonic modes are theoretically investigated in a graphene-loaded waveguide surrounded by indium antimonide (InSb) and magnetized plasma layers operating in the GHz frequency regime. The dispersion relation is derived using transfer matrix technique and the conductivity of graphene is modeled using the Kubo formalism. Hybrid plasmon modes are observed due to the presence of anisotropic plasma. The influence of material parameters such as chemical potential (μ_c), cyclotron frequency (ω_c), plasma frequency (ω_p), relaxation time (τ), number of graphene layers (N), and temperature (T) on effective mode index (EMI) and graphene's conductivity are numerically analyzed. Numerical results show that the variations in graphene's chemical potential and relaxation time significantly influence the EMI and cutoff frequencies. Higher chemical potential (μ_c) increases the cutoff frequency and enhances plasmonic coupling. Furthermore, tensorial permittivity of magnetized plasma parameters i.e., cyclotron frequency and plasma frequency play crucial role in modulating the dispersion curves and shift the plasmonic frequencies. The temperature-dependent permittivity of InSb provides an additional degree of freedom for tuning electromagnetic (EM) wave propagation. These findings may have potential applications in tunable plasmonic devices, optical devices related to surface plasmon polaritons (SPPs) by using plasma, and thermal photonic devices.

Introduction

With the rapid advancement in optical techniques, there is a continuous exploration for the integration of highly efficient photonic technologies intended for data transmission and communication systems [1]. These optical technologies include silicon photonics, lithium niobate photonics, indium phosphide photonics, and plasmonics [2, 3]. The rate of data transmission increases by reducing the element size of the photonic devices up to the nanometer (nm) scale. However, it becomes very difficult for conventional photonic devices to reduce the element size up to nanometer scale due to diffraction limit of light [4]. Plasmonics has emerged as a highly promising solution by the excitation of surface plasmon polaritons (SPPs), for next generation electronic-photonic integration, due to its ability to confine and manipulate light below the diffraction limit. These exceptional features of SPPs allow the integration of ultra-compact devices with high speed data transfer capacity, low energy consumption, and enhanced bandwidth. SPPs have become a promising candidate for light sources to control the propagation and dispersion of light at nanometer scale [5]. SPPs are characterized by strong field confinement close to the interface [6, 7].

Subwavelength confinement of SPPs offers an effective way to promote photonics and chip electronics technology in which light signals propagate in nanophotonic devices at optical frequency regime. Plasmonic technology undergoes a revolution by the emergence of 2D optical materials that offers new ideas to explore photonic and electronic properties [8]. Graphene has attracted significant scientific attention due to its exceptional physical properties, exhibiting promising potential for applications in optoelectronic and nano-electronic devices. Graphene exhibits ultra-high electron mobility, gate-variable optical conductivity, and ultrafast relaxation time for photo-excited carriers [9]. Graphene also possesses incredible optical properties such as strong light-matter interaction, high speed and broadband operation etc [10]. Graphene is an outstanding candidate for designing tunable optical devices that operates in both optical and GHz frequency ranges due to its tunable conductivity and charge carrier density. Moreover, the tunable conductivity of graphene opens new doors for tunable optical sensors, tunable GHz absorber, and tunable metamaterials [11, 12]. Graphene provides a way for controlling the optical bistability by appropriately varying the applied voltage [13]. Graphene plasmon polaritons show strong field confinement as well as relatively long propagation distance as compared to plasmon polaritons in noble metals [14]. A lot of research has been conducted on graphene and isotropic materials. However, isotropic materials lack polarization sensitivity and less control over dispersion characteristics.

The efficiency of graphene-based devices can be enhanced by integrating them with magnetized plasma. Plasma, when integrated with graphene exhibits exceptional characteristics. Generally, plasma is considered to be unmagnetized when no external magnetic field is applied [15] but as the external magnetic field is applied, an anisotropic behavior is induced in plasma. This behavior is used to manipulate the SPPs, offering a greater control compared to unmagnetized plasma [16]. Numerous theoretical investigations have highlighted the role of plasma medium to study the characteristics of SPPs [17-26]. Xu et al. analyzed experimentally and theoretically the wavelength of SPPs at the dielectric-plasma interface [27]. Shahmansouri et al. examined the collective excitation of SPs in a massless Dirac plasma by using a relativistic quantum fluid model [28]. Furthermore, plasma-based waveguide offers a novel approach to nanophotonic devices. Plasmonic modes in graphene-loaded waveguide surrounded by InSb and magnetized plasma layers have not been explored in the existing literature.

The objective of this study is to theoretically model graphene-loaded waveguide surrounded by magnetized plasma and indium antimonide (InSb) for thermal control of SPPs. Indium antimonide (InSb), a small bandgap semiconducting material has emerged as a temperature sensitive material in the field of plasmonics and nano-photonics, which can significantly guide the SPPs at various temperatures [29]. Optical properties of InSb are highly responsive to temperature variations, making it an ideal candidate for GHz technology [29-31]. Furthermore, InSb can be fabricated with standard fabrication techniques which make it easier to incorporate into practical devices. In the present study, we will investigate the impact of material parameters by plotting dispersion relation to compute effective mode index (EMI) and graphene's conductivity in the interested frequency regime. The proposed geometry will allow strong light-matter coupling, enhance field confinement, and tunable plasmon modes which will lead towards highly efficient optical devices.

Methodology

The theoretical modelling of the graphene-loaded waveguide surrounded by magnetized plasma and InSb is presented in this section. Figure 1 illustrates the propagation of EM waves along z-direction.

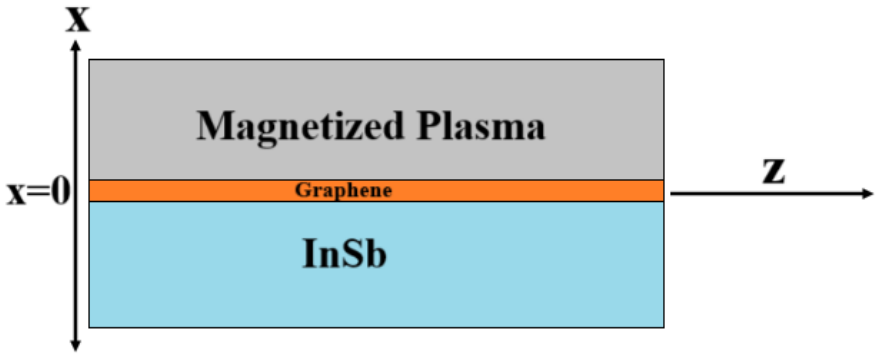

Figure 1: schematic view of graphene-loaded waveguide surrounded by InSb and magnetized plasma.

Graphene's conductivity is modelled using the Kubo formula.

$$\sigma(g) = \frac{ie^2(\omega - j2\tau)}{\pi\hbar^2} \times \left[\frac{1}{(\omega - j2\tau)^2} \int_0^\infty \xi_{en} \times \left(\frac{\partial f_d(\xi_{en})}{\partial \xi_{en}} - \frac{\partial f_d(-\xi_{en})}{\partial \xi_{en}} \right) d\xi_{en} - \int_0^\infty \frac{f_d(-\xi_{en}) - f_d(\xi_{en})}{(\omega - j2\tau)^2 - 4\left(\frac{\xi_{en}}{\hbar}\right)^2} d\xi_{en} \right] \quad 1$$

$f_d(\xi_{en}) = \left(e^{(\xi_{en} - \mu_c)/K_B T} + 1\right)^{-1}$ is the Fermi-Dirac distribution. where μ_c, τ, T, e, K_B, ω, ξ_{en} and $\hbar$ are chemical potential, relaxation rate, temperature, charge on electron, Boltzmann's constant, operating frequency, energy, and reduced Plank's constant, respectively [32].

Magnetized plasma has the following constitutive relations:

$$D = \varepsilon_0 \bar{\bar{\varepsilon}} E \quad 2$$

$$H = 1/\mu_0 B \quad 3$$

μ_0 and ε_0 represent the permeability and permittivity of free space, respectively, and $\bar{\bar{\varepsilon}}$ is the tensorial permittivity tensor for anisotropic plasma.

$$[\bar{\bar{\varepsilon}}] = \begin{bmatrix} \varepsilon_1 & -i\varepsilon_2 & 0 \\ i\varepsilon_2 & \varepsilon_1 & 0 \\ 0 & 0 & \varepsilon_3 \end{bmatrix} \quad 4$$

Where, ε_1, ε_2 and ε_3 represent the tensorial permittivity of plasma medium as reported in [19] and $\varepsilon_1 = \varepsilon_0\left(1 - \frac{(\omega_p)^2}{(\omega)^2 - (\omega_c)^2}\right)$, $\varepsilon_2 = \varepsilon_0\left(\frac{\omega_c * (\omega_p)^2}{\omega * ((\omega)^2 - (\omega_c)^2)}\right)$, $\varepsilon_3 = \varepsilon_0\left(1 - \frac{(\omega_p)^2}{(\omega)^2}\right)$, $\omega_p = \sqrt{\frac{ne^2}{m\,\varepsilon_0}}$, $\omega_c = \frac{eB}{m}$. ω_c, ω_p represent the cyclotron frequency and plasma frequency [17]. $e, B, m, n,$ and ε_0 represent the electron charge, magnetic field, electron mass, number density of electrons, and permittivity of free space, respectively [33]. The wave equation for H_z and E_z in the magnetized plasma are as follows [16]:

$$[\nabla^2 E_{z1}\ \nabla^2 H_{z1}] + [U_1\ iU_2\ iU_3\ U_4][E_{z1}\ H_{z1}] = 0 \quad 5$$

Where,

$$\nabla = \hat{e}_x \frac{\partial}{\partial x} + \hat{e}_y \frac{\partial}{\partial y} + \hat{e}_z \frac{\partial}{\partial z} \quad 6$$

$$U_1 = -\left(\frac{\beta^2 \varepsilon_3}{\varepsilon_1} - \omega^2 \mu_0 \varepsilon_3\right) \quad 7$$

$$U_2 = \frac{\omega \mu_0 \beta \varepsilon_2}{\varepsilon_1} \quad 8$$

$$U_3 = -\beta \omega \varepsilon_2 \frac{\varepsilon_3}{\varepsilon_1} \quad 9$$

$$U_4 = \frac{(\omega^2 \mu_0 \varepsilon_1^2 - \omega^2 \mu_0 \varepsilon_2^2)}{\varepsilon_1} - \beta^2 \quad 10$$

Where, β and μ_0 denote the propagation constant and permeability of free space, respectively. Model fields for magnetized plasma are given as:

$$E_{z1} = (A_1 e^{-q_1 x} + A_2 e^{-q_2 x}) e^{-i\beta z} \quad 11$$

$$H_{z1} = i(A_1 \alpha_1 e^{-q_1 x} + A_2 \alpha_2 e^{-q_2 x})\, e^{-i\beta z} \quad 12$$

The remaining magnetized plasma field components can be derived from [34].

$$E_t = ia\nabla_t E_z + b\nabla_t E_z \times a_z + c\nabla_t H_z + id\nabla_t H_z \times a_z \quad 13$$

$H_t = e\nabla_t E_z + if\nabla_t E_z \times a_z + ia\nabla_t H_z + b\nabla_t H_z \times a_z$ 14

Where a, b, c, d, e and f are given by [16]

$a = \frac{U_3\omega\mu_0\varepsilon_2 - U_4\beta\varepsilon_3}{\varepsilon_1(U_1U_4+U_2U_3)}$ 15

$b = -\frac{U_3\omega\mu_0}{U_1U_4+U_2U_3}$ 16

$c = -\frac{U_1\omega\mu_0\varepsilon_2+U_2\beta\varepsilon_3}{\varepsilon_1(U_1U_4+U_2U_3)}$ 17

$d = -\frac{U_1\omega\mu_0}{U_1U_4+U_2U_3}$ 18

$e = -\frac{U_3\beta}{(U_1U_4+U_2U_3)}$ 19

$f = \frac{U_4\omega\varepsilon_3}{(U_1U_4+U_2U_3)}$ 20

The eigenvalues are:

$k_1 = \sqrt{\frac{1}{2}(U_1+U_4)+\frac{1}{2}\sqrt{(U_1-U_4)^2-4U_2U_3}}$ 21

$k_2 = \sqrt{\frac{1}{2}(U_1+U_4)-\frac{1}{2}\sqrt{(U_1-U_4)^2-4U_2U_3}}$ 22

The associated eigen functions describe the hybrid nature of SPPs:

$q_1 = \sqrt{\beta^2 - {k_1}^2}$ 23

$q_2 = \sqrt{\beta^2 - {k_2}^2}$ 24

α_1 and α_2 describe hybrid mode factors [17].

$\alpha_1 = \frac{U_1-{q_1}^2}{U_2}$ 25

$\alpha_2 = \frac{U_1-{q_2}^2}{U_2}$ 26

InSb EM fields components are given as:

$E_{y2} = A_3\, e^{\gamma_1 x}$ 27

$H_{y2} = A_4\, e^{\gamma_1 x}$ 28

$E_{z2} = \frac{i\gamma_1}{\omega\varepsilon_{InSb}}(A_4 e^{\gamma_1 x})$ 29

$H_{z2} = -\frac{i\gamma_1}{\omega\mu_0}(A_3 e^{\gamma_1 x})$ 30

Where, $\varepsilon_{InSb} = \varepsilon_\infty - \frac{\omega_p^2}{\omega^2+i\gamma\omega}$, ω_p describe the plasma frequency, $\omega_p = \sqrt{\frac{nq^2}{0.015\varepsilon_0 m_e}}$, $q = -1.60\times10^{-19}C$ charge on electron, $m_e = 9.11\times10^{-31}$ kg electron mass, relative permittivity $\varepsilon_\infty = 15.68$, damping constant $\gamma = \pi\times10^{11}\ rad\ s^{-1}$, carrier density $n = 5.76\times10^{20}T^{\frac{3}{2}}exp(-\frac{E_g}{2K_BT})$, where E_g is the bandgap of value $E = 0.26eV$ and K_B is Boltzmann constant, $K_B = 8.62\times10^{-5}\ eV\ K^{-1}$. $\gamma_1 = \sqrt{\beta^2-\omega^2\varepsilon_{InSb}\mu_0}$ is permittivity of InSb medium [29].

In all calculation $e^{-i\beta z}$ is omitted. A_1, A_2, A_3 and A_4 are amplitudes constant. Using anisotropic plasma and InSb fields components following boundary conditions are applied.

$\hat{x}\times(H_1 - H_2) = \sigma E$ 31

$\hat{x}\times(E_1 - E_2) = 0$ 32

Where, σ is the graphene's surface conductivity

The obtained dispersion relation is:

$$i\Big(\gamma_1\big(\mu_0\omega q_1(f+b\alpha_1)\alpha_2-(b^2+df)(-i\mu_0\sigma\omega+\gamma_1)q_1q_2(-\alpha_1+\alpha_2)-\mu_0\omega q_2\alpha_1(f+b\alpha_2)\big)-(\varepsilon_{InSb}\omega+i\sigma\gamma_1)\big((-i\mu_0\sigma\omega+\gamma_1)q_1(b-d\alpha_1)+\mu_0\omega(\alpha_1-\alpha_2)-(-i\mu_0\sigma\omega+\gamma_1)q_2(b-d\alpha_2)\big)\Big)=0 \quad (33)$$

Results and Discussion

In this section, numerical analysis of proposed planar structure is analyzed in the interested frequency region. The numerical analytical results are discussed by using dispersion relation 33. The results are examined by computing dispersion curves, effective mode index (EMI), and conductivity of graphene as a function of GHz frequency to observe the behavior of SPPs. Two types of SPPs modes i.e., lower, and higher mode confirm hybrid nature of plasma medium. In all calculations the numerical parameters are set as: ω_c=6 *THz*, ω_p=2×10^{13}Hz, T=280K, τ=8ps and μ_c=0.3*eV*. Figure 2 presents the EMI as the function of incident wave frequency (GHz), for different values of chemical potential (μ_c). The chemical potential in graphene controls the position of the Fermi level, which in turn affects the charge carrier concentration [35-38]. In lower frequency mode, the EMI increases rapidly with frequency for all values of the chemical potential. For highest chemical potential i.e., μ_c=0.9 *eV*, EMI increases more steeply and reaches higher values, implying stronger coupling and enhanced mode confinement. At lowest chemical potential μ_c=0.1 *eV*, the increase in the EMI is less pronounced, meaning weaker coupling and less confinement. At lower frequencies, the chemical potential directly impacts the carrier density in graphene, which governs the plasma frequency. At higher frequencies, the chemical potential has less influence on the effective mode index. This is because the graphene behavior shifts from plasmonic response to more dielectric-like response. The increase in effective mode index becomes less sensitive to changes in chemical potential as the frequency rises above the plasmon resonance. In the high-frequency region, the plasmonic effects diminish, and the graphene's behavior is more influenced by its dielectric properties rather than its conductivity. As a result, the EMI starts to stabilize. Hence graphene's response at these higher frequencies is less dependent on chemical potential. Lower mode is beneficial for plasmonic devices, communication systems, and GHz sensors, where the chemical potential in graphene can be tuned to control mode confinement and enhance signal propagation. In case of higher propagating mode, as the frequency increases, the EMI increases with the increase in incident wave frequency. Figure 3 depicts the variation in EMI versus incident wave frequency under different values of relaxation time. In case of lower propagating mode, for lowest value of relaxation time, the EMI increases quickly and reaches higher values as reported in [39, 40]. This is because shorter relaxation times lead to higher carrier scattering rates, which results in stronger plasmonic effects and thus a stronger mode confinement. As the relaxation time is increased, the dispersion curves moves towards lower frequency region. In case of higher propagating mode, the EMI increase with increasing relaxation time but the effect of relaxation time disappears at higher frequency values indicating non-physical region which has no significance in scientific community. Additionally, higher relaxation time shift the dispersion curves to lower cutoff frequencies in both propagating modes which is validated from the literature [38].

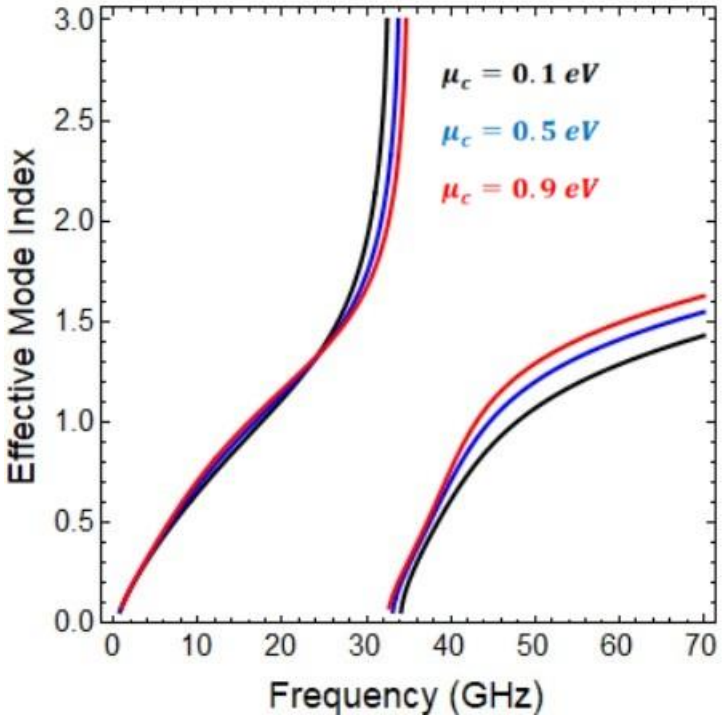

Figure 2: Influence of graphene's chemical potential on EMI versus GHz frequency.

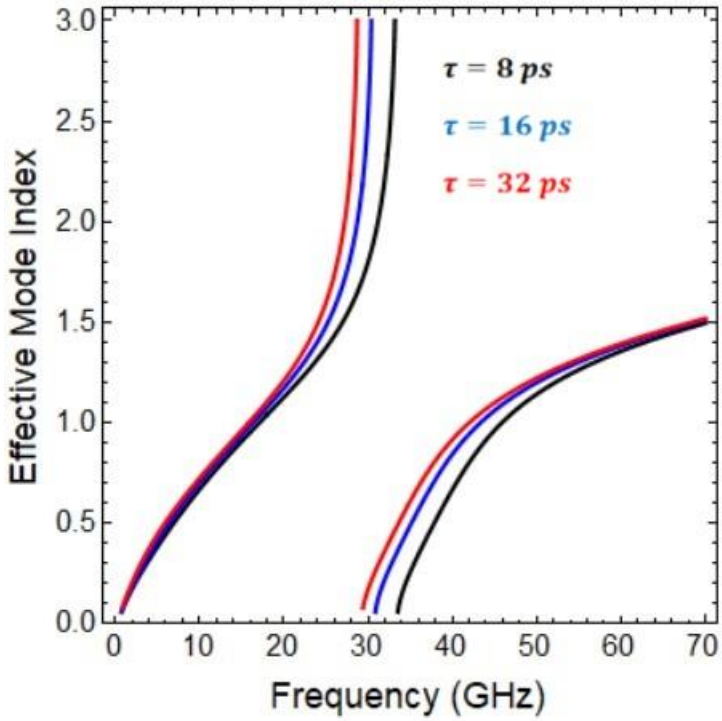

Figure 3: Influence of graphene's relaxation time on EMI versus GHz frequency.

The dependence of EMI on number of graphene layers as a function of incident wave frequency is depicted in figure 4. In case of lower mode, the EMI increases steeply with frequency for all values of N. For N=1, the increase in the EMI is the steepest, indicating stronger coupling and tighter mode confinement. Because single layer graphene has higher surface-to-volume ratio, which results in stronger plasmonic effects enable high-speed communication systems like fiber optics or microwave photonics and increasing N changes the modal coupling and field distribution. The electromagnetic waves interact more strongly

with the charge carriers in the graphene, leading to better mode confinement and higher effective mode index. The EMI increases with increasing incident wave frequency as the number of graphene layer increase. For upper propagating mode, the EMI increases as a function of incident wave frequency as the number of graphene layers is increased. It is also observed that the frequency band start squeezing as the number of graphene layers are increased. These tunable features of graphene may be useful for future fabrication of nano-photonic devices in the plasmonic community [41].

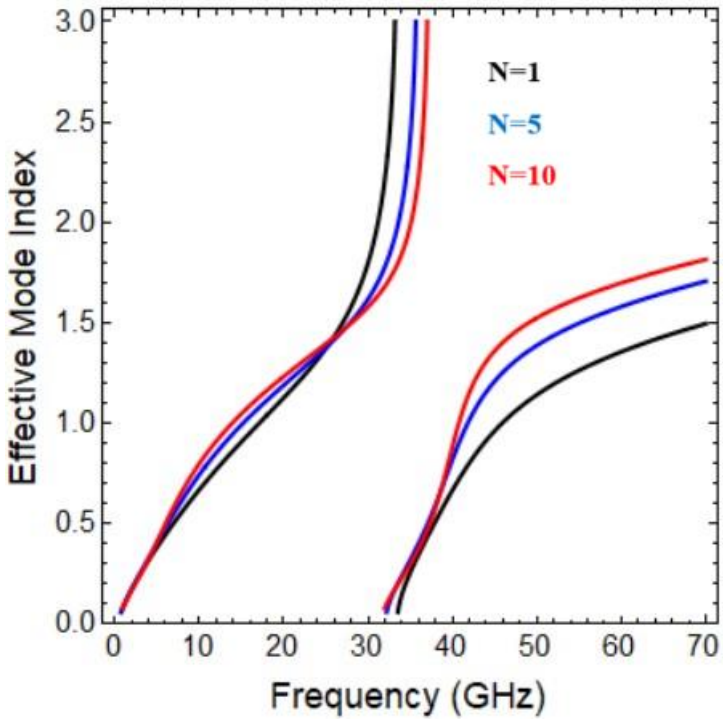

Figure 4: Influence of graphene's layers on EMI versus GHz frequency.

The influence of plasma frequency on EMI versus incident wave frequency is analyzed in figure 5. For lower propagating mode, the EMI increases with frequency for all values of ω_p, indicating that the plasmonic modes became more confined. Increasing plasma frequency modifies the tensor permittivity components which strengthen electromagnetic confinement. It is observed that when the plasma frequency increases, EMI increases and the curves move towards lower frequency regime. The plasma frequency is a function of number density of electrons which exhibits significant role in tunable plasmon modes. It is of peculiar of interest to note that at lower frequencies (below ~20 GHz), the EMI increases slowly. Consequently, at lower frequencies, the plasma's effect on the waveguide is less significant, and the wave propagates more freely. When the frequency increases over 20 GHz, there is drastic increase in EMI. This shows that the plasma influence becomes more pronounced as the frequency increases, leading to stronger confinement of SPPs. The EMI increases with increasing plasma frequency as a function of incident wave frequency for higher propagating mode. The understanding of the behavior of plasmonic modes is crucial to design plasmonic waveguides. These results offer promising potential for designing tunable high frequency waveguides and are consistent with literature [40]. Figure 6 illustrates the effect of cyclotron frequency on EMI as a function of incident wave frequency. In lower propagating mode, the EMI curves rises rapidly at low cyclotron frequency. As the cyclotron frequency rises, the corresponding EMI curve increases smoothly with increasing wave frequency and the propagating mode bandgap start squeezing. Moreover, the effect of cyclotron frequency disappears after 30 GHz and the region become non-significant region. The EMI start decreasing with increasing value of incident wave frequency, as the

cyclotron frequency increases. This behavior is crucial for GHz plasmonic applications where precise control of wave propagation is important for improving the device performance.

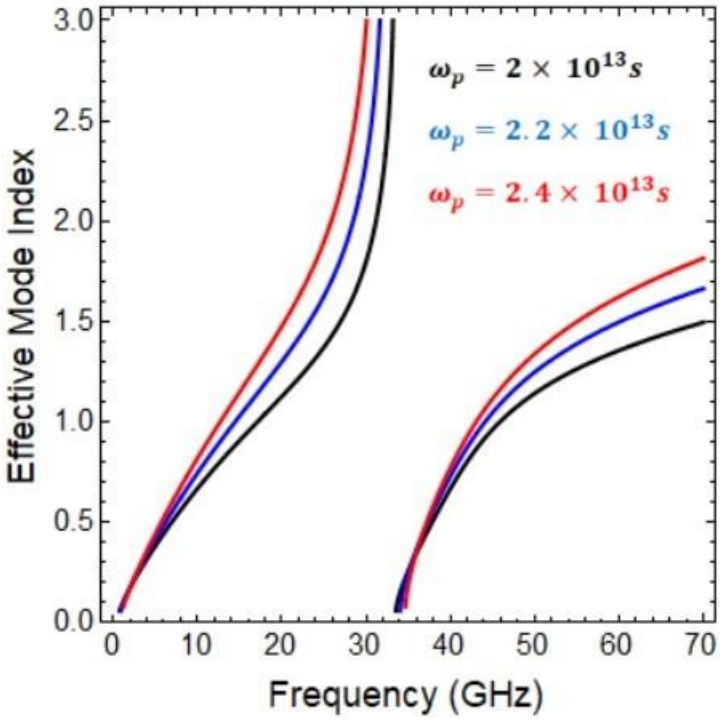

Figure 5: Influence of plasma frequency on EMI versus GHz frequency.

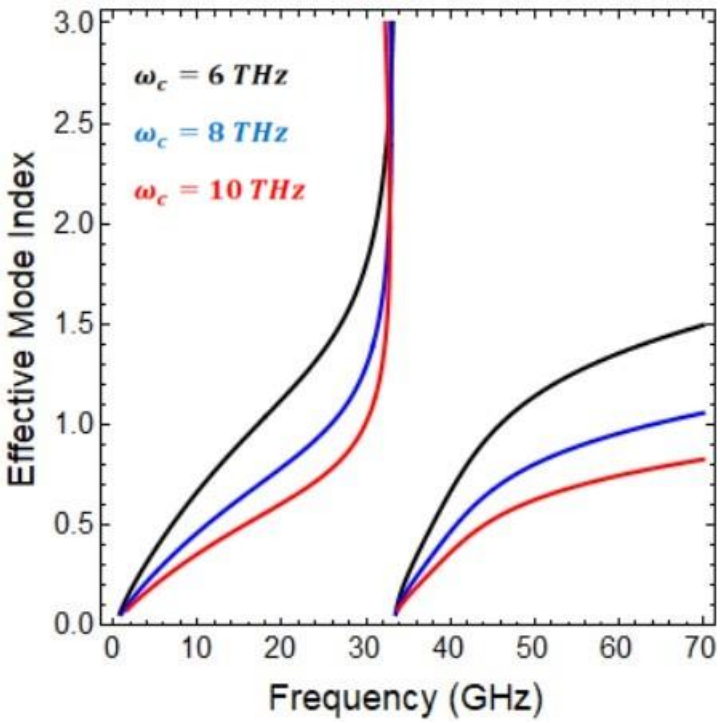

Figure 6: Influence of cyclotron frequency on EMI versus GHz frequency.

The influence of InSb temperature on EMI as a function of incident frequency is illustrated in figure 7. In lower propagating mode, as the temperature of InSb increases, the corresponding EMI curve shifts towards higher frequency region. Temperature variation modifies the carrier concentration and mobility in InSb, which in turn alters its plasma frequency and effective permittivity. The temperature of InSb exhibits

strong influence on upper propagating mode, EMI increases as the temperature increases and the bandgap starts squeezing. This behavior is important for thermo-plasmonic applications where the temperature dependence of plasmonic properties is critical. Higher values of temperature lead towards strong plasmon coupling and higher energy excitation in plasmonic devices, which affect their performance in applications, such as sensing and imaging. This temperature sensitivity plays an important role in system efficiency and response. The variation in surface conductivity of graphene versus GHz waves frequency under different plasma frequencies is analyzed in figure 8. As the plasma frequency of the magnetized plasma increases, there is a sharp increase in conductivity and the curves shifts towards lower frequency region. Additionally, the frequency band of both modes begins to squeeze as the plasma frequency increases. The conductivity of graphene sharply decreases near the plasma frequency of the magnetized plasma, making it valuable for applications such as graphene-based metamaterials. The dependence of graphene's conductivity under different cyclotron frequencies is studied in figure 9. As the cyclotron frequency increases, the conductivity increases and curves shifts towards higher frequency region. This is because the interaction between the electrons in graphene and the electromagnetic field becomes more pronounced at higher cyclotron frequencies. Plasma characteristics have strong influence on the modulation and propagation of hybrid SPPs for the proposed geometry which can be utilized for potential applications such as nanophotonic and optoelectronic devices in GHz frequency regime. Figure 10 demonstrated how InSb temperature influences the interaction between the incident wave and the graphene's conductivity. As the temperature of InSb increases, it influences the graphene's conductivity by affecting the electron mobility and the interaction between graphene and electromagnetic waves. Higher temperatures typically lead to increased electron scattering, which reduces the conductivity of graphene. Based on numerical results, it can be inferred that temperature-sensitive sensors can be developed by leveraging the variation in graphene's conductivity to detect temperature changes in the surrounding environment.

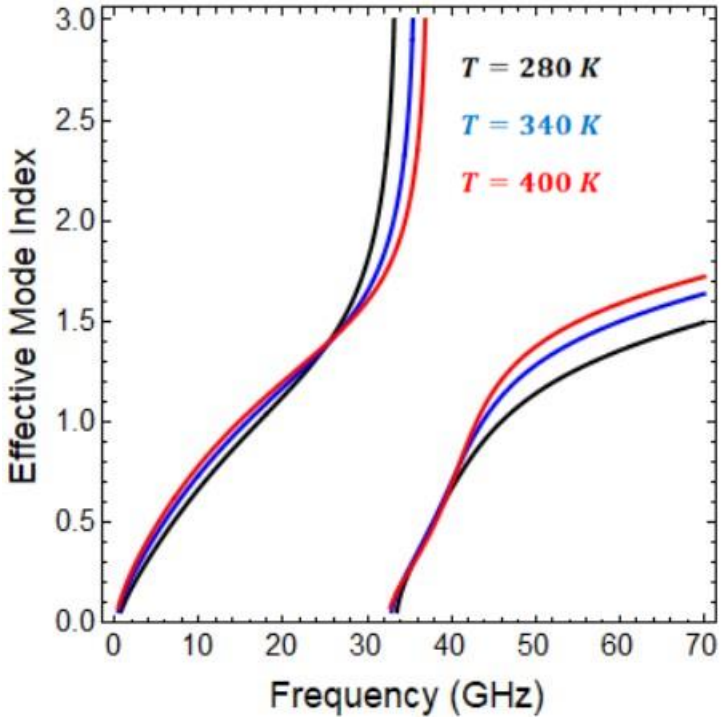

Figure 7: Influence of InSb temperature on EMI versus GHz frequency.

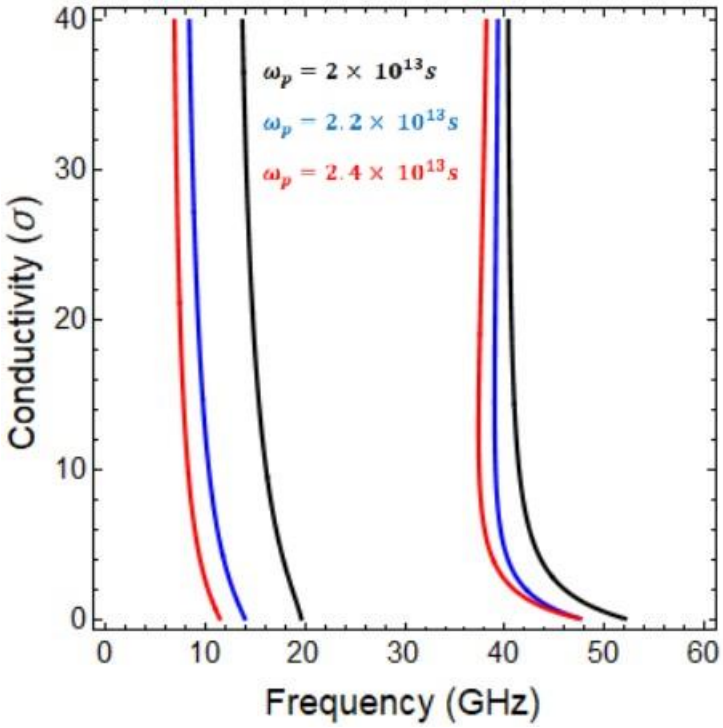

Figure 8: Influence of plasma frequency on graphene's conductivity versus GHz frequency.

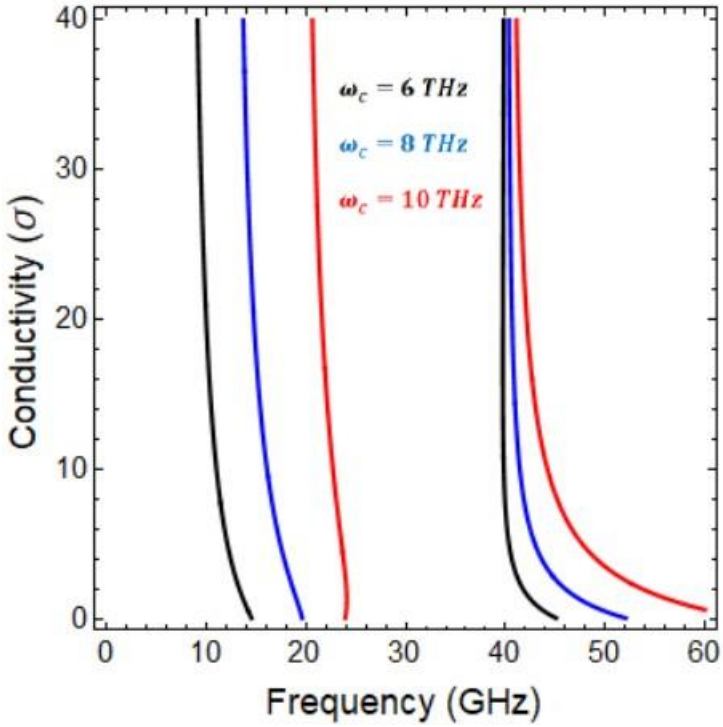

Figure 9: Influence of cyclotron frequency on graphene's conductivity versus GHz frequency.

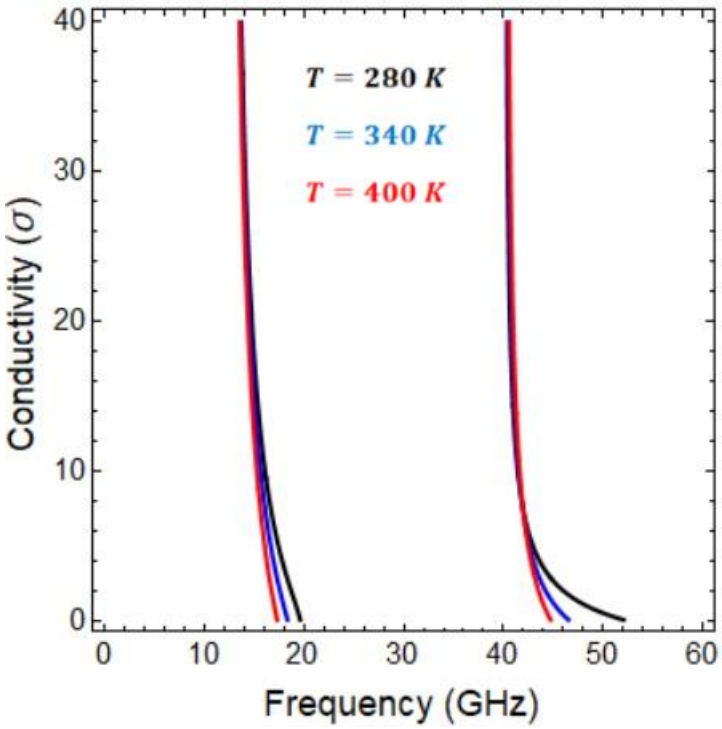

Figure 10: Influence of InSb temperature on graphene's conductivity versus GHz frequency.

Conclusion

This study presented a theoretical model to analyze the hybrid plasmonic modes in graphene-loaded waveguide surrounded by InSb and magnetized plasma. The extended wave theory is used to derive the electromagnetic (EM) field components and transfer matrix technique is used to obtain the dispersion relation. The conductivity of graphene is modeled using Kubo formula. The influence of chemical potential, relaxation time, number of graphene layers, plasma frequency, cyclotron frequency, and InSb temperature on effective mode index and graphene's conductivity is analyzed numerically. Based on the numerical results, the material parameters reveal significant insights into the SPPs properties. Due to the anisotropic nature of the magnetized plasma, two plasmon modes (lower and upper modes) are observed which exhibit different behaviors in lower and higher frequency regions. Moreover, the influence of material parameters on effective mode index and graphene's conductivity highlights the sensitivity of SPPs in the interested frequency regime. The present work offers promising potential for application in high performance and tunable plasmonic devices, including optical modulators, tunable plasmonic antennas, GHz sensors, and thermal photonic devices.

Funding: Funding is inappropriate for this research study.
Data availability: The statistics supporting the outcomes of this research are accessible upon reasonable request from the first author.

Declarations

Ethical approval: Not applicable
Consent to participate: Not applicable
Consent to publish: All authors have given consent to publish.
Competing interest: The authors have no competing interests to declare.

References

1. Li, K., et al., *Electronic–photonic convergence for silicon photonics transmitters beyond 100 Gbps on–off keying.* Optica, 2020. **7**(11): p. 1514-1516.
2. Chen, P.-K., et al., *Adapted poling to break the nonlinear efficiency limit in nanophotonic lithium niobate waveguides.* Nature Nanotechnology, 2024. **19**(1): p. 44-50.
3. Haffner, C., et al., *All-plasmonic Mach–Zehnder modulator enabling optical high-speed communication at the microscale.* Nature Photonics, 2015. **9**(8): p. 525-528.
4. Li, K., et al., *An integrated CMOS–silicon photonics transmitter with a 112 gigabaud transmission and picojoule per bit energy efficiency.* Nature Electronics, 2023. **6**(11): p. 910-921.
5. Elshaari, A.W., et al., *Hybrid integrated quantum photonic circuits.* Nature photonics, 2020. **14**(5): p. 285-298.
6. Schröter, U. and A. Dereux, *Surface plasmon polaritons on metal cylinders with dielectric core.* Physical Review B, 2001. **64**(12): p. 125420.
7. Zhang, J., L. Zhang, and W. Xu, *Surface plasmon polaritons: physics and applications.* Journal of Physics D: Applied Physics, 2012. **45**(11): p. 113001.
8. Umair, M., et al., *Tunability of plasmon modes at uniaxial chiral–black phosphorus planar structure.* Plasmonics, 2024: p. 1-9.
9. Novoselov, K.S., et al., *Electric field effect in atomically thin carbon films.* science, 2004. **306**(5696): p. 666-669.
10. Castro Neto, A.H., et al., *The electronic properties of graphene.* Reviews of modern physics, 2009. **81**(1): p. 109-162.
11. Liu, M., et al., *A graphene-based broadband optical modulator.* Nature, 2011. **474**(7349): p. 64-67.
12. Bonaccorso, F., et al., *Graphene photonics and optoelectronics.* Nature photonics, 2010. **4**(9): p. 611-622.
13. Xiang, Y., et al., *Tunable optical bistability at the graphene-covered nonlinear interface.* Applied Physics Letters, 2014. **104**(5).
14. Xiao, S., et al., *Graphene-plasmon polaritons: From fundamental properties to potential applications.* Frontiers of Physics, 2016. **11**(2): p. 117801.
15. Umair, M., et al., *Modelling of Surface Plasmon Polaritons (SPPs) in Magnetized Plasma-Graphene-PEMC Interfaces.* Plasmonics, 2025: p. 1-8.
16. Umair, M., et al., *Plasmonic modes of metallic slab in anisotropic plasma environment.* Plasmonics, 2023. **18**(5): p. 1857-1864.
17. Ali, M., et al., *Study of hybrid surface Plasmon modes in metallic circular waveguide filled with magnetized plasma.* Waves in Random and Complex Media, 2022. **32**(1): p. 449-462.
18. Ali, R., B. Zamir, and H. Shah, *Transverse electric surface waves in a plasma medium bounded by magnetic materials.* Results in physics, 2018. **8**: p. 243-248.
19. Alkanhal, M.A., et al., *Propagation of hybrid surface waves in ferrite anisotropic plasma planar structures.* Optik, 2021. **229**: p. 166255.
20. Ivanov, S. and N. Nikolaev, *Magnetic-field effect on wave dispersion in a free semiconductor plasma slab.* Journal of Physics D: Applied Physics, 1999. **32**(4): p. 430.
21. Shaban, M., et al., *Plasmonic characteristics of LiF filled slab waveguide in isotropic plasma environment.* Plasmonics, 2024: p. 1-7.
22. Shaban, M., et al., *Tunable characteristics of light plasmon coupling in Lithium Fluoride (LiF) sandwiched waveguide structure bounded by plasma and graphene layers.* Plasmonics, 2024: p. 1-7.
23. Umair, M., et al., *Transverse electric surface waves in ferrite medium surrounded by plasma layers.* Journal of the European Optical Society-Rapid Publications, 2020. **16**: p. 1-6.

24. Umair, M., et al., *Dispersion characteristics of hybrid surface waves at chiral-plasma interface.* Journal of Electromagnetic Waves and Applications, 2021. **35**(2): p. 150-162.
25. Yaqoob, M., et al., *Electromagnetic scattering from perfect electromagnetic conductor cylinders placed in magnetized plasma medium.* Optoelectronics and Advanced Materials-Rapid Communications, 2014. **8**(November-December 2014): p. 1150-1156.
26. Zamir, B. and R. Ali, *Characteristics of TE surface waves in a plasma medium bounded by nonlinear metamaterials.* Journal of the Korean Physical Society, 2018. **72**: p. 1166-1173.
27. Xu, X., et al., *Visual phenomena of surface plasmon polaritons at the dielectric-plasma interface.* Applied Physics Letters, 2008. **92**(1).
28. Shahmansouri, M., R. Aboltaman, and A. Misra, *Surface plasmons in a semi-bounded massless Dirac plasma.* Physics Letters A, 2018. **382** (32): p. 2133-2136.
29. Yaqoob, M., et al., *Thermally tunable electromagnetic surface waves supported by graphene loaded indium antimonide (InSb) interface.* Scientific Reports, 2023. **13**(1): p. 18631.
30. Sajid, M., et al., *Modeling of graphene wrapped indium antimonide nanowire as thermo-optical waveguide.* Materials Research Express, 2025. **12**(3): p. 036201.
31. Zhang, C., et al., *Design of a highly sensitive terahertz temperature and refractive index composite sensor based on an InSb–Ag composite grating.* Journal of the Optical Society of America B, 2024. **41**(2): p. 411-420.
32. Falkovsky, L. and A. Varlamov, *Space-time dispersion of graphene conductivity.* The European Physical Journal B, 2007. **56**: p. 281-284.
33. Umair, M., et al., *Characteristics of Plasmon Mode at Anisotropic Plasma–Black Phosphorene Interface.* Plasmonics, 2024: p. 1-8.
34. Gong, J., *Electromagnetic wave propagation in a chiroplasma-filled waveguide.* Journal of plasma physics, 1999. **62**(1): p. 87-94.
35. Arif, M., et al., *Dispersion properties in uniaxial chiral–graphene–uniaxial chiral plasmonic waveguides.* Plasmonics, 2024: p. 1-10.
36. Mahal, A., et al., *Characteristics of Photon–Plasmon Coupling in Uniaxial Chiral Filled Slab Waveguide Bounded by Graphene Layers.* Plasmonics, 2025. **20**(3): p. 1473-1480.
37. Shaban, M., et al., *Light Plasmon Coupling in Graphene-Wrapped Cylindrical Waveguide Filled with Lithium Fluoride (LiF).* Plasmonics, 2025: p. 1-8.
38. Umair, M., et al., *Hybrid plasmon modes at chiroferrite-graphene interface.* Plasmonics, 2024. **19**(4): p. 2193-2199.
39. Azam, M., et al., *Dispersion characteristics of surface plasmon polaritons (SPPs) in graphene–chiral–graphene waveguide.* Waves in Random and Complex Media, 2021: p. 1-12.
40. Umair, M., et al., *Plasmonic characteristics of monolayer graphene in anisotropic plasma dielectric.* Plasmonics, 2024. **19**(3): p. 1165-1171.
41. Umair, M., et al., *Light plasmon coupling in planar chiroplasma–graphene waveguides.* Plasmonics, 2023. **18**(3): p. 1029-1035.